Differentiation between G3 pancreatic neuroendocrine tumor and pancreatic neuroendocrine carcinoma based on intratumor and peritumor CT value ratio and abnormal vascular network

Chaoyang Zhang*† and Wei Hao†

Department of Radiology, Jincheng General Hospital, Jincheng, Shanxi, China

Background: To develop a model based on computed tomography (CT) images to differentiate between grade 3 (G3) pancreatic neuroendocrine tumors (pNETs) and pancreatic neuroendocrine carcinoma (pNECs).

Methods: This retrospective study included patients with pathologically confirmed pNETs and pNECs who underwent abdominal CT examinations at JINCHENG GENERAL Hospital between June 2012 and June 2023. Tumor and peri-tumor CT characteristics were assessed, including peri-tumor areas A (0−10 mm) and B (10−20 mm) during the arterial and portal venous phases of dynamic enhancement. A model was established using binary logistic regression and receiver operating characteristic (ROC) curves.

Results: A total of 42 patients were included: 20 with G3 pNETs and 22 with pNECs. The ROC analysis showed that the combination of the arterial phase CT ratio B1, portal venous phase CT ratio B2, pancreatic duct invasion (PDI), peripancreatic fat infiltration (PFI), and abnormal vascular network (AVN) [area under the ROC curve (AUC)=0.970 (95% confidence interval (CI): 0.927-1.000), sensitivity=95.50%, and specificity=90.00%] exhibited a better performance in identifying G3 pNETs and pNECs than the combination of the arterial phase CT ratio B1 and the portal venous phase CT ratio B2 [AUC = 0.907 (95% CI: 0.818-0.996), sensitivity=77.30%, and specificity=95.00%], and the combination of arterial phase CT ratio B1, portal venous phase CT ratio B2, and AVN [AUC = 0.923 (95% CI: 0.810-1.000), sensitivity=81.80%, and specificity=85.00%].

Conclusion: The enhancement ratio between the tumor and peri-tumoral B area in the arterial and portal venous phases, along with AVN, PFI, and PDI, may serve as effective indicators for distinguishing pNECs from G3 pNETs.

Introduction

Pancreatic neuroendocrine neoplasms (pNENs) exhibit significant heterogeneity and various biological characteristics (1). The different hormones secreted by pNENs can lead to a wide variety of clinical symptoms among patients (2, 3). Low-grade pNENs often display an indolent growth pattern, whereas high-grade pNENs are invasive and tend to metastasize early (4). In recent years, the incidence of pNENs has significantly increased due to advancements in examination technology, allowing the detection of smaller tumors (5). According to the World Health Organization (WHO) 2019 classification standards, pNENs can be classified into grade G1-G3-grade pancreatic neuroendocrine tumors (pNETs) and pancreatic neuroendocrine carcinomas (pNECs) (6). G3 pNETs and pNECs are distinct entities with overlapping features that complicate diagnosis, yet differ in pathology (7–10), treatment strategies (7–10), and prognosis (11–15). G3 pNETs may benefit from therapies used for lower-grade NETs (alkylating agents, somatostatin analogs, targeted therapies), and responses to platinum-based chemotherapy are generally poor (16–19). pNECs, conversely, show greater response to platinum-based regimens (cisplatin/etoposide) typical for high-grade carcinomas (16, 20, 21). Hence, the precise differentiation between G3 pNETs and pNECs is crucial.

Still, differentiating between G3 pNETs and pNECs is not easy. Pathologically, Distinguishing G3 pNETs from pNECs is difficult due to shared proliferation indices (Ki67 > 20%), leading to diagnostic ambiguity in some cases despite immunohistochemistry and molecular testing (22), and more aggressive histopathological features (23), but biopsies can be unreliable since they sample only a small part of the tumor that can be unrepresentative of the whole tumor, and waiting for surgery and the pathological examination of the specimen can lead to missed therapeutic opportunities (22). Ideally, the early differentiation between pNETs and pNECs should be based on imaging since it is non-invasive and can be performed early in the course of the disease. Magnetic resonance imaging (MRI) can differentiate between pNETs and pNECs (24), but MRI has accessibility, availability, and cost issues, particularly in developing countries. Computed tomography (CT) is the first-line imaging modality in patients suspected of pNENs, but it has a lower resolution than MRI for soft tissues (25). CT-based models have been developed successfully for the differential diagnosis of pNETs and pancreatic duct adenocarcinoma (PDAC), either using age, pancreatic duct dilatation, and portal enhancement ratio (26), or CA 19–9 levels, tumor shape, and pancreatic duct dilation (27), but pNECs were not included, while another model (tumor margin, enhanced degree, parenchymal atrophy, and texture parameters) could differentiate between pNECs and PDAC but did not include pNETs (28). Two studies in pNENs showed that some CT texture features could differentiate different tumor types (29, 30). Nevertheless, pNENs are rare tumors, and a CT-based model differentiating between G3 pNETs and pNECs is lacking.

It was hypothesized that pNETs and pNECs display significant differences in the relationships among the tumor, pancreatic duct, and peripancreatic fat, the abnormal vascular network (AVN) surrounding the tumor, and the enhancement ratio between tumor and normal tissues. This study aimed to determine a model based on CT images to differentiate between pNETs and pNECs based on those features. The results could help improve the diagnosis of pNETs vs. pNECs and patient management.

Materials and methods

Study design and patients

This retrospective study collected patients with pNEN who underwent abdominal CT examination at the JINCHENG GENERAL Hospital between June 2012 and June 2023. This study was approved by the ethics committee of the JINCHENG GENERAL Hospital (approval #LL2024032101). The requirement for individual consent was waived due to the retrospective nature of the study. The inclusion criteria were 1) pathological diagnosis of G3 grade PNET or PNEC, 2) did not receive any anti-tumor treatment before abdominal CT examination, 3) CT image quality was satisfactory, clearly displaying the lesion and surrounding areas, and 4) complete medical data. The exclusion criteria were 1) the CT images contained severe artifacts or noise that affected measurement, or 2) the biopsy or surgical pathology results indicated G1 or G2 pNET.

Data collection and definitions

Image acquisition

During the entire study period, an Optima 680 CT instrument (GE Healthcare, Waukesha, WI, USA) was used to conduct a thorough scan of the abdomen, ranging from the top of the diaphragm to the level of the renal hilum. The routine parameters were tube voltage of 120 kV, tube current of 250 mA, pitch of 0.992, field of view of 360 mm, matrix of 512×512, and layer thickness and layer spacing of 3 mm. After the initial scan, 100 mL of the contrast agent (iopromide, 240 mgI/ml) was injected through the cubital vein at a flow rate of 2.5 mL/s. When the CT value of the abdominal aorta reached 100 HU, the arterial phase scan was initiated automatically, and the portal vein scan was conducted 70 s later.

Image analysis

Two experienced radiologists used the Picture Archiving and Communication System (PACS) to analyze and interpret the images. In case of disagreement, a decision was reached through discussion and agreement. Tumor size, tumor location, tumor composition, calcification, pancreatic duct invasion (PDI), peripancreatic fat infiltration (PFI), and AVN were determined. PDI was defined as the distal expansion of the main pancreatic duct near the lesion. PFI was defined as the peripancreatic fat being unclear and not smooth. AVN was defined as an abnormally proliferating vascular network surrounding the tumor.

When measuring the CT values, the tumor body and two specific areas around the tumor (A and B zones) were included, while the cystic necrosis regions in the tumor body and the non-pancreatic tissues were excluded. The tumor area was manually delineated, and zones A and B were automatically delineated by the CT system. The CT value of necrotic/cystic areas within the tumor generally ranges from 10 to 20 HU, and they do not enhance during any phase of enhancement. The first area, called peritumoral A, refers to the region between the tumor edge and a distance of 10 mm surrounding it. The second area, referred to as peritumoral B, extends from 10 to 20 mm surrounding the tumor edge, excluding non-pancreatic tissues. A region of interest (ROI) with an area of 10 mm^2 was manually outlined, and the CT values of the tumor and peritumoral areas were measured in the arterial and portal venous phases. These values were measured thrice to calculate the average. The tumor and portal venous phase values were finally calculated in the arterial and portal venous phases, respectively. The enhancement ratio of the peritumoral A area (CT ratio A1, A2) and the enhancement ratio of the tumor body to the peritumoral B area (CT ratio B1, B2) were also determined as follows. CT ratio A1=arterial phase A-zone CT value ÷ arterial phase tumor CT value. CT ratio B1=arterial phase B-zone CT value ÷ arterial phase tumor CT value. CT ratio A2=venous phase A-zone CT value ÷ venous phase tumor CT value. CT ratio B2=venous phase B-zone CT value ÷ venous phase tumor CT value.

Statistical analysis

SPSS 25.0 (IBM, Armonk, NY, USA) was used to perform the statistical analysis. The continuous data following a normal distribution were expressed as means ± standard deviations and analyzed using Student's t-test. The categorical data were presented as n (%) and analyzed using the chi-squared test or Fisher's exact probability test. The continuous and categorical data were analyzed using univariable logistic regression to identify useful indicators for distinguishing G3 grade pNETs and pNECs. A multivariable binary logistic regression model was constructed to evaluate its discriminant performance. The variables with P<0.05 in the univariable analyses and those with clinical significance were included in the multivariable binary logistic regression analysis (enter method). A receiver operating characteristic (ROC) curve analysis was performed to determine the performance of the model, based on the area under the curve (AUC). An agreement test was performed to determine the intraclass coefficient (ICC) between the two radiologists. Two-sided P-values <0.05 were considered statistically significant.

Results

Characteristics of the patients

The 42 patients included 21 males and 21 females, aged between 27 and 75 years, with an average age of 54.74 ± 12.10. There were 20 patients in the G3 pNET group and 22 patients in the pNEC group. In the G3 pNET group, there were 12 males and eight females,

ranging in age from 27 to 73 years, with an average age of 53.65 ± 13.39 years. In the pNEC group, there were nine males and 13 females, ranging in age from 32 to 75 years, with an average age of 55.73 ± 11.00 years. There were no significant differences in age, sex, tumor size, calcification, composition, arterial phase, and portal venous phase A area enhancement ratio (CT ratio A1, A2) between the two groups (all P>0.05). However, there were statistically significant differences in PDI, PFI, AVN, and arterial and portal venous phase enhancement ratios (CT ratios B1 and B2) (all P<0.05) (Table 1, Figure 1).

In addition, the agreement test showed that the CT value of the tumor in arterial stage (ICC = 0.946), peritumor area A in arterial stage (ICC = 0.983), peritumor B area in arterial stage (ICC = 0.989), tumor in venous stage (ICC = 0.979), peritumor area A in venous stage (ICC = 0.986), and peritumor B area in venous stage (ICC = 0.979) examined by the two radiologists had a favorable consistency (Supplementary Table S1). The overall conformity was ICC = 0.951.

Constructing the model

The univariable logistic regression analyses showed that PDI, PFI, AVN, and portal venous phase CT ratios could be used to differentiate G3 pNETs from pNECs (Tables 2, 3). Patients in the NEC group exhibited a higher frequency of tumors with PDI (odds ratio (OR)=2.203, 95% confidence interval (CI): 1.078-4.505), PFI (OR = 2.551, 95%CI: 1.160-5.618), and AVN (OR = 2.841, 95%CI: 1.395-5.208) (Table 2). The AUCs of arterial phase and portal

TABLE 1 Comparison of the general information and CT characteristics between the G3 grade NET group and NEC group.

Features	G3 NET (n=20)	NEC (n=22)	t/χ^2	P
Age, years	53.65 ± 13.39	55.73 ± 11.00	-0.551	0.585
Sex, M (F)	12 (8)	9 (13)	1.527	0.354
Size, mm	55.20 ± 45.67	44.0 ± 26.0	0.941	0.352
Solid (cystic)	20 (0)	18 (4)	4.019	0.109
Calcification	1	2	0.264	0.607
PFI	7	17	7.644	<0.05
PDI	7	16	6.019	<0.05
AVN	2	14	12.780	0.001
Arterial phase				
CT ratio A1	0.72 ± 0.10	0.71 ± 0.10	0.276	0.784
CT ratio B1	0.79± 0.12	0.68± 0.08	3.470	0.001
Venous Phase				
CT ratio A2	0.83± 0.07	0.79± 0.09	1.601	0.117
CT ratio B2	1.05 ± 0.10	0.88 ± 0.10	5.487	<0.001

G3 NET, grade 3 neuroendocrine tumor; NEC, neuroendocrine carcinoma; M, male; F, female; PFI, peripancreatic fat infiltration; PDI, pancreatic duct invasion; AVN, abnormal vascular network; CT, computed tomography.
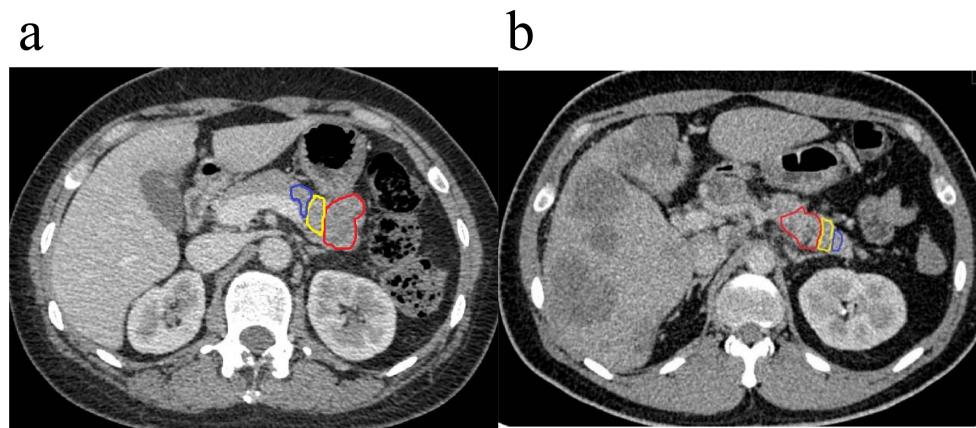
FIGURE 1
Region of interest (ROI) delineated in axial portal phase computed tomography (CT). **(a)** A 63-year-old male patient was diagnosed with G3 pancreatic neuroendocrine tumor (pNET) at the tail of the pancreas, and the space between the adjacent gastric body fat had disappeared. **(b)** A 34-year-old male patient presented with pancreatic neuroendocrine carcinoma (pNEC) in the pancreatic body, with the tumor invading the nearby splenic artery, showing rough and localized narrowing, multiple intrahepatic metastases, and peritoneum multiple enlarged lymph nodes (the red area is the tumor body, the yellow area is peritumor **(a)** the blue area is peritumor **(b)**.

venous phase CT ratios for distinguishing G3 pNETs from pNECs were 0.791 (95%CI: 0.645-0.937) and 0.902 (95%CI: 0.812-0.993), respectively. When the arterial phase CT ratio cutoff value was 0.759, the sensitivity and specificity were 75.00% and 81.80%, respectively. When the portal venous phase CT ratio cutoff value was 0.914, the sensitivity and specificity were 95.00% and 72.70%, respectively (Table 3, Figure 2).

The ROC analysis showed that the combination of the arterial phase CT ratio B1, portal venous phase CT ratio B2, PDI, PFI, and AVN (AUC = 0.970, 95%CI: 0.927-1.000, sensitivity of 95.50%, and specificity of 90.00%) exhibited a better performance in identifying G3 pNETs and pNECs than the combination of the arterial phase CT ratio B1 and the portal venous phase CT ratio B2 (AUC = 0.907, 95% CI: 0.818-0.996, sensitivity of 77.30%, and specificity of 95.00%), and the combination of arterial phase CT ratio B1, portal venous phase CT ratio B2, and AVN (AUC = 0.923, 95% CI: 0.810-1.000, sensitivity of 81.80%, and specificity of 85.00%) (Table 4, Figure 3).

Discussion

This retrospective study built models based on CT images to differentiate between G3 pNETs and pNECs. The results suggested

that the enhancement ratio between the tumor and peritumoral B area in the arterial and portal venous phases, AVN, PFI, and PDI, could serve as an indicator for effectively distinguishing pNECs from G3 pNETs.

The present study revealed no statistically significant differences between patients with G3 pNETs vs. pNECs in terms of demographic (age and sex), histological (tumor size and calcification), and imaging (composition, arterial phase, and portal venous phase CT ratio A) characteristics, consistent with the study by Belousova et al. (31).

The present study employed a diagnostic approach combining quantitative and qualitative analysis. By combining the arterial phase CT ratio B1 and the portal venous phase CT ratio B2, the study aimed to detect intra-pancreatic PDI, PFI, and AVN. These factors were combined to establish a multivariable binary logistic regression model to develop a reliable method for distinguishing between pNECs and G3 pNETs.

Recent studies indicated that distinguishing between the two can be effectively accomplished by considering the arterial and portal venous phases of CT ratios B1 and B2, which have been identified as autonomous predictive factors (29, 30). It could be because higher-grade PNETs have lower tumor angiogenesis than lower-grade PNETs, consistent with the WHO 2017 classification system (32, 33). A previous study on the grading of pNETs was consistent with the WHO 2019 classification system and pathological analysis (6) and was similar to two previous studies on arterial and portal vein enhancement rates (34, 35). The previous studies relied on specific cutoff values of arterial and portal vein enhancement rates to identify G1, G2, and G3 pNETs, respectively, and to identify G1, G2, and G3 pNETs and pNECs. However, the measured CT values did not consider the presence of peritumoral edema and adjacent pancreatic tissue. Due to invasion and other factors, the peritumoral area was not divided into different regions, and the inconsistent CT values in different areas surrounding the

TABLE 2 Univariate logistic regression analysis of G3 grade NET group and NEC group 1 (*n* = 42).

Features	β	SE	P	OR	95%CI
PDI	1.949	0.892	<0.05	2.203	1.078-4.505
PFI	1.624	0.884	<0.05	2.551	1.160-5.618
AVN	2.739	1.089	<0.05	2.841	1.395-5.208

SE, standard error; OR, odds ratio; CI, confidence interval; PDI, pancreatic duct invasion; PFI, peripancreatic fat infiltration; AVN, abnormal vascular network.

TABLE 3 Univariate logistic regression analysis of G3 grade NET group and NEC group 2 (*n* = 42).

CT ratio	AUC	Sensitivity	Specificity	Cut point
CT ratio B1	0.791 (95%CI: 0.645, 0.937)	75.00%	81.80%	0.759
CT ratio B2	0.902 (95%CI: 0.812, 0.993)	95.00%	72.70%	0.914

AUC, area under the curve; CT, computed tomography; CI, confidence interval.

TABLE 4 Multivariable binary logistic regression analysis of G3 grade NET group and NEC group (*n* = 42).

Combination Model	AUC	Sensitivity	Specificity	Cut point
Model 1	0.907 (95%CI: 0.818, 0.996)	77.30%	95.00%	0.735
Model 2	0.923 (95%CI: 0.841, 1.000)	81.80%	85.00%	0.683
Model 3	0.970 (95%CI: 0.927, 1.000)	95.50%	90.00%	0.432

AUC, area under the curve; CT, computed tomography; CI, confidence interval; PFI, peripancreatic fat infiltration; PDI, pancreatic duct invasion; AVN, abnormal vascular network; CT, computed tomography.
Model 1, arterial phase CT ratio B1 and portal venous phase CT ratio B2.
Model 2, arterial phase CT ratio B1, portal venous phase CT ratio B2, and AVN.
Model 3, arterial phase CT ratio B1, portal venous phase CT ratio B2, PDI, PFI, and AVN.

tumor were not properly analyzed and documented. In this study, the tumor area was finely divided into the peritumoral zone A, closer to the lesion (0–10 mm), and the peritumoral zone B, farther from the lesion (10–20 mm). The CT values of the pancreatic lesion and the adjacent tissue are commonly affected by unstable factors such as peritumoral edema, inflammation, necrosis, and adjacent tissue invasion (36, 37); therefore, the CT value of zone B (i.e., 10-20-mm peritumoral) was measured because it was hypothesized to be less likely affected by peritumoral edema, inflammation, necrosis, and adjacent tissue invasion. The present study considered the fact that the CT value remained relatively stable in the peritumoral B area, located far from the lesion, compared with the tumor body and peritumoral A area, and pNECs and G3 pNETs can be distinguished based on their CT ratio.

Then, based on the univariable logistic regression model, pNECs exhibited a higher propensity for PDI compared with G3 pNETs, as well as higher frequencies of PFI and AVN. G3 pNETs infrequently invade the main pancreatic duct (MPD); when present,

intraductal extension is considered a unique and rare growth pattern. On the other hand, pNECs are more aggressive, with rapid progression and a higher frequency of invasion into adjacent tissues, including the ductal system (23, 24, 38). The extent and pattern of PFI on imaging (CT/MRI) help differentiate the more aggressive, poorly differentiated pNEC from G3 pNETs, though overlap exists, especially in advanced tumors (39–42). Both tumor types can infiltrate surrounding fat, but pNECs are
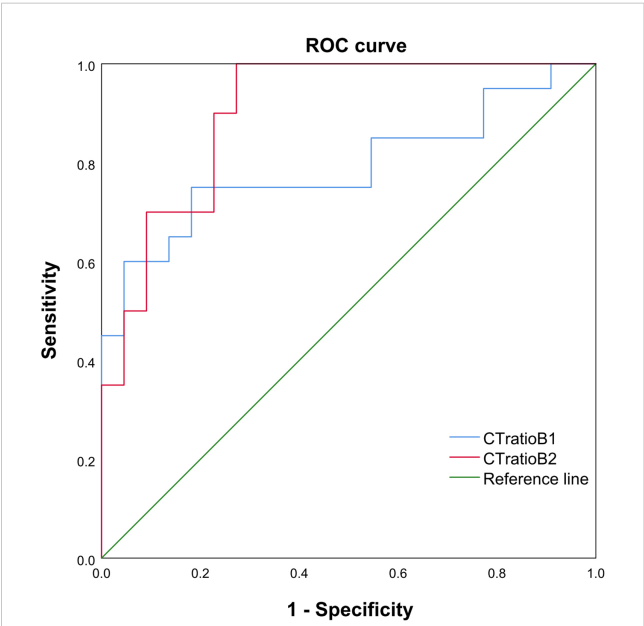

FIGURE 2
The receiver operating characteristics (ROC) curve, cut point value, and corresponding sensitivity as well as specificity of each cut point value of CT ratio B1 and CT ratio B2 between pNECs and G3 grade (pNETs). The areas under the curve (AUCs) for CT ratio B1 and B2 were 0.791 (95% CI: 0.645, 0.937) and 0.902 (95% CI: 0.812, 0.993), respectively. The sensitivity and specificity were found to be the highest for CT ratio B2 <0.914.

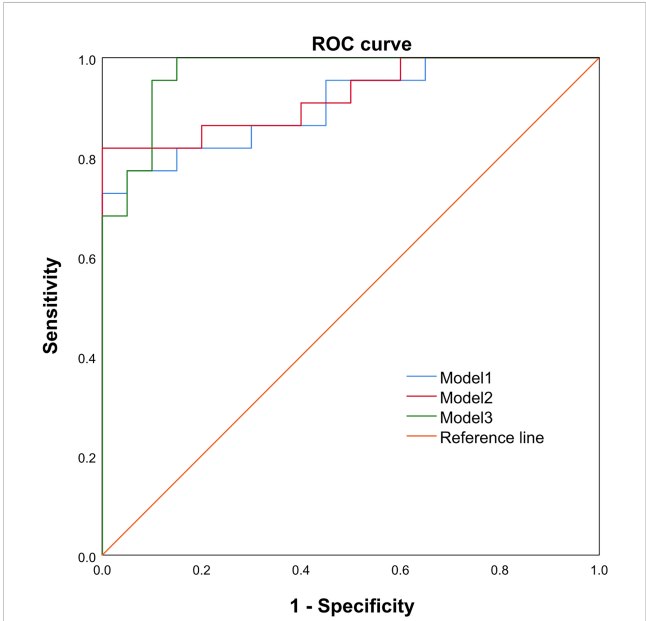FIGURE 3
The ROC curve, cut point value, and corresponding sensitivity, as well as the specificity of each cut point value of Models 1, 2, and 3 between pNEC and G3 grade pNET. The AUCs for Models 1, 2, and 3 were 0.907 (95%CI: 0.818, 0.996), 0.923 (95%CI: 0.841, 1.000), and 0.970 (95%CI: 0.927-1.000), 95.50% and 90.00%, respectively. The sensitivity and specificity were the highest for Model 3.

characterized by higher grade, poor differentiation, and worse prognosis, resulting in more frequent extensive infiltration beyond the pancreas (39, 40). Regarding AVN, G3 pNETs often preserve a well-organized, organoid vascular network that is characteristic of well-differentiated neuroendocrine cells, including abundant neurosecretory granules and relatively uniform vessel distribution (23, 43). G3 pNECs typically display more chaotic, disorganized, and poorly formed vasculature, reflecting their poorly differentiated cytology and aggressive biological behavior (22, 23, 43). All three features (PDI, PFI, and AVN) can be observed on enhanced CT images.

At present, the diagnosis, identification, and prediction of G3 pNETs and pNECs are based on diverse imaging techniques and methods such as dynamic enhanced CT and MRI gray-scale ratio, histogram analysis, radiomics, deep learning, and transfer learning (44–47). In addition, there is currently an increasing emphasis on assessment. For example, De Robertis et al. (48) analyzed the apparent diffusion coefficient (ADC) value of tumors and used histograms to predict tumor invasiveness. Analyzing pNEN histograms on ADC maps could aid in predicting tumor grade, vascular invasion, lymph nodes, and liver metastases in pNENs. The most precise indicators for detecting pNENs with aggressive tendencies are ADC entropy and ADC kurtosis. They concluded that ADC entropy and ADC peak were the most reliable variables for distinguishing pNENs displaying malignant characteristics. In another study, Li et al. (49) examined radiomics features based on MRI images and could effectively predict the grade of pNETs. Their findings suggested that higher grades of pNETs were associated with increased metastasis risk and unfavorable prognosis. Xu et al. (24) reported that MRI could differentiate between pNETs and pNECs. Indeed, MRI has high sensitivity but has inconveniences like accessibility, availability, and cost, especially in developing countries (50, 51). Hence, CT could be more appropriate than MRI for the workup of pNENs. Nevertheless, limited information exists regarding the application of the observation of the peritumoral vascular network, peritumoral divisions, and CT ratios of the tumor body and peritumoral area during the arterial phase and portal venous phase for the differential diagnosis of G3 pNETs and pNECs. In this study, by examining the various characteristics of the tumor and peritumoral areas, measuring and calculating the average CT value of the ROI in the solid area of the tumor and the peritumoral B area, and the ratio of each phase after enhancement, accurate and dependable indicators were identified for distinguishing between the two tumor types.

Strengths and limitations

A strength of this study is the use of CT images that were consistently obtained using the same scanner among all patients and analyzed uniformly by the same two radiologists. Still, this study has limitations. The study was performed at a single center, and the sample size was small since G3 pNETs and pNECs are relatively rare tumors. Still, the sample size in the present study compares with previous ones (29, 35, 49). The study was retrospective and limited to the images and data found in the patient charts. Although a model was successfully built and displayed a high AUC (0.970), no external validation was performed. There is no widely accepted anatomical or biological justification in the literature for dividing pancreatic peritumoral zones specifically into 0–10 mm (zone A) and 10–20 mm (zone B); these boundaries are arbitrary and not based on robust anatomical or tumor biology data (52–56). Still, cutoffs had to be determined and tried, and those are the ones tried in the present study. Finally, due to the available data and the small sample size, the model developed here could not be compared against other models based on KI67, histopathology, or MRI. Additional studies are necessary to confirm the study findings.

Clinical significance

Abdominal enhanced CT is a first-line imaging examination method for pNEN (1, 25–27, 29, 31, 34, 46). In this study, AVN, PDI, and PFI were observed, and the ratio of enhanced CT tumor body to peritumoral CT values was calculated to differentiate G3 grade pNET from pNEC. The AVN, PDI, PFI, and the ratio of arterial/portal venous phase to plain CT values can objectively reflect the nature of the tumor, and the magnitude of their changes was associated with the degree of tissue infiltration around the tumor and the presence of distant metastasis. The CT measurements of pancreatic tumors and the surrounding tissues are frequently influenced by variable factors, including swelling around the tumor, inflammation, tissue death, and infiltration into adjacent structures (36, 37); therefore, the CT value of zone B (i.e., 10-20-mm peritumoral) was measured. The results showed that the CT ratios B1 and B2 in the arterial and portal venous phases were higher in the pNET group than in the pNEC group (P<0.001 for both). Considering that the median survival time of G3 grade pNET patients is 41–99 months, while that of pNEC patients is only 8–13 months (11–15), and considering that the treatment strategies for the two diseases are different (7–10), the clinical significance is that accurately distinguishing G3 grade pNET from pNEC using the commonly-used enhanced CT examination is important in terms of patient management, avoid under- or over-treatment, and prognosis determination.

Conclusion

The results suggest that the CT ratio of the tumor and peritumoral B area, AVN, PDI, and PFI can be combined into a model to differentiate between G3 pNETs and pNECs with a high diagnostic performance.

Data availability statement

The original contributions presented in the study are included in the article/Supplementary Material. Further inquiries can be directed to the corresponding author.

Ethics statement

This study was approved by the Ethics Committee of Jincheng General Hospital (LL2024032101). The studies were conducted in accordance with the local legislation and institutional requirements. Written informed consent for participation was not required from the participants or the participants' legal guardians/next of kin in accordance with the national legislation and institutional requirements.

Author contributions

CZ: Writing – original draft. WH: Writing – original draft.

Funding

The author(s) declare that no financial support was received for the research, and/or publication of this article.

Conflict of interest

The authors declare that the research was conducted in the absence of any commercial or financial relationships that could be construed as a potential conflict of interest.

Generative AI statement

The author(s) declare that no Generative AI was used in the creation of this manuscript.

Any alternative text (alt text) provided alongside figures in this article has been generated by Frontiers with the support of artificial intelligence and reasonable efforts have been made to ensure accuracy, including review by the authors wherever possible. If you identify any issues, please contact us.

Publisher's note

All claims expressed in this article are solely those of the authors and do not necessarily represent those of their affiliated organizations, or those of the publisher, the editors and the reviewers. Any product that may be evaluated in this article, or claim that may be made by its manufacturer, is not guaranteed or endorsed by the publisher.

Supplementary material

The Supplementary Material for this article can be found online at: https://www.frontiersin.org/articles/10.3389/fonc.2025.1616763/full#supplementary-material

References

1. Lee NJ, Hruban RH, Fishman EK. Pancreatic neuroendocrine tumor: review of heterogeneous spectrum of CT appearance. *Abdom Radiol (NY)*. (2018) 43:3025–34. doi: 10.1007/s00261-018-1574-4

2. Taboada R, Claro L, Felismino T, de Jesus VH, Barros M, Riechelmann RP. Clinicopathological and molecular profile of grade 3 gastroenteropancreatic neuroendocrine neoplasms. *J Neuroendocrinol*. (2022) 34:e13099. doi: 10.1111/jne.13099

3. Takayanagi D, Cho H, Machida E, Kawamura A, Takashima A, Wada S, et al. Update on epidemiology, diagnosis, and biomarkers in gastroenteropancreatic neuroendocrine neoplasms. *Cancers (Basel)*. (2022) 14(5). doi: 10.3390/cancers14051119

4. Zhu JK, Wu D, Xu JW, Huang X, Jiang YY, Edil BH, et al. Cystic pancreatic neuroendocrine tumors: A distinctive subgroup with indolent biological behavior? A systematic review and meta-analysis. *Pancreatology*. (2019) 19:738–50. doi: 10.1016/j.pan.2019.05.462

5. Wu W, Chen J, Bai C, Chi Y, Du Y, Feng S, et al. The Chinese guidelines for the diagnosis and treatment of pancreatic neuroendocrine neoplasms (2020). *J Pancreatol*. (2021) 4:1–17. doi: 10.1097/jp9.0000000000000064

6. Jirasek T, Mandys V. Changes in histopathological classification of neuroendocrine tumors in 5th edition of WHO classification of gastrointestinal tract tumors (2019). *Cesk Patol*. (2020) 56:207–11.

7. Donadio MD, Brito AB, Riechelmann RP. A systematic review of therapeutic strategies in gastroenteropancreatic grade 3 neuroendocrine tumors. *Ther Adv Med Oncol*. (2023) 15:17588359231156218. doi: 10.1177/17588359231156218

8. Das S, Dasari A. Epidemiology, incidence, and prevalence of neuroendocrine neoplasms: are there global differences? *Curr Oncol Rep*. (2021) 23:43. doi: 10.1007/s11912-021-01029-7

9. Kaliszewski K, Ludwig M, Greniuk M, Mikula A, Zagorski K, Rudnicki J. Advances in the diagnosis and therapeutic management of gastroenteropancreatic neuroendocrine neoplasms (GEP-NENs). *Cancers (Basel)*. (2022) 14(8). doi: 10.3390/cancers14082028

10. Cives M, Pelle E, Strosberg J. Emerging treatment options for gastroenteropancreatic neuroendocrine tumors. *J Clin Med*. (2020) 9(11). doi: 10.3390/jcm9113655

11. Jiang J, Park J, Kim S, Daan A, Donahue T, Girgis MD. Surgical resection of high-grade nonfunctional pancreatic neuroendocrine carcinoma is associated with improved survival. *J Surg Oncol*. (2021) 124:1373–80. doi: 10.1002/jso.26644

12. Feng T, Lv W, Yuan M, Shi Z, Zhong H, Ling S. Surgical resection of the primary tumor leads to prolonged survival in metastatic pancreatic neuroendocrine carcinoma. *World J Surg Oncol*. (2019) 17:54. doi: 10.1186/s12957-019-1597-5

13. Luo W, Zhang T. Primary tumor resection enhances the survival of pancreatic neuroendocrine carcinoma patients with liver metastasis under the definition of 2019 WHO classification. *J Cancer Res Clin Oncol*. (2023) 149:9201–12. doi: 10.1007/s00432-023-04847-3

14. Lee L, Ito T, Jensen RT. Prognostic and predictive factors on overall survival and surgical outcomes in pancreatic neuroendocrine tumors: recent advances and controversies. *Expert Rev Anticancer Ther*. (2019) 19:1029–50. doi: 10.1080/14737140.2019.1693893

15. Zhang WH, Wang WQ, Gao HL, Xu SS, Li S, Li TJ, et al. Tumor-infiltrating neutrophils predict poor survival of non-functional pancreatic neuroendocrine tumor. *J Clin Endocrinol Metab*. (2020) 105(7). doi: 10.1210/clinem/dgaa196

16. Raj N, Valentino E, Capanu M, Tang LH, Basturk O, Untch BR, et al. Treatment response and outcomes of grade 3 pancreatic neuroendocrine neoplasms based on morphology: well differentiated versus poorly differentiated. *Pancreas*. (2017) 46:296–301. doi: 10.1097/mpa.0000000000000735

17. Boutin M, Mathews A, Badesha J, Paul A, Safro M, Gill S, et al. Well-differentiated grade 3 neuroendocrine tumors: characteristics, treatments, and outcomes from a population-based study. *Pancreas*. (2022) 51:756–62. doi: 10.1097/mpa.0000000000002100

18. Hinterleitner M, Pfeiffer R, Trautwein NF, Sipos B, Singer S, Nadalin S, et al. Treatment modalities favoring outcome in well-differentiated neuroendocrine tumors G3. *Front Endocrinol*. (2024) 14:1285529. doi: 10.3389/fendo.2023.1285529

19. Liu AJ, Ueberroth BE, McGarrah PW, Buckner Petty SA, Kendi AT, Starr J, et al. Treatment outcomes of well-differentiated high-grade neuroendocrine tumors. *Oncol*. (2021) 26:383–8. doi: 10.1002/onco.13686

20. Jann H, Kayser A, Wiedenmann B, Tacke F, Roderburg C. Treatment outcomes of patients with G3 neuroendocrine neoplasms. *J Clin Oncol*. (2020) 38:622–2. doi: 10.1200/JCO.2020.38.4_suppl.622

21. Sorbye H, Welin S, Langer SW, Vestermark LW, Holt N, Osterlund P, et al. Predictive and prognostic factors for treatment and survival in 305 patients with advanced gastrointestinal neuroendocrine carcinoma (WHO G3): The NORDIC NEC study. *Ann Oncol.* (2013) 24:152–60. doi: 10.1093/annonc/mds276

22. Chen J, Wu W, Bai C, Chi Y, Huo L, Jiang L, et al. Consensus on the clinical diagnosis and treatment of grade 3 pancreatic neuroendocrine tumors. *J Pancreatol.* (2024) 7:97–105. doi: 10.1097/jp9.0000000000000183

23. Zhang MY, He D, Zhang S. Pancreatic neuroendocrine tumors G3 and pancreatic neuroendocrine carcinomas: Differences in basic biology and treatment. *World J Gastrointest Oncol.* (2020) 12:705–18. doi: 10.4251/wjgo.v12.i7.705

24. Xu W, Zhang H, Feng G, Zheng Q, Shang R, Liu X. The value of MRI in identifying pancreatic neuroendocrine tumour G3 and carcinoma G3. *Clin Radiol.* (2021) 76:551 e1–9. doi: 10.1016/j.crad.2021.02.031

25. Dromain C, Deandreis D, Scoazec JY, Goere D, Ducreux M, Baudin E, et al. Imaging of neuroendocrine tumors of the pancreas. *Diagn Interv Imaging.* (2016) 97:1241–57. doi: 10.1016/j.diii.2016.07.012

26. Hu M, Lv L, Dong H. A CT-based diagnostic nomogram and survival analysis for differentiating grade 3 pancreatic neuroendocrine tumors from pancreatic ductal adenocarcinomas. *Front Oncol.* (2024) 14:1443213. doi: 10.3389/fonc.2024.1443213

27. Chen HY, Zhang XY, Deng XY, Ge YL, Tang YQ, Cui H, et al. Grade 3 pancreatic neuroendocrine tumors on MDCT: establishing a diagnostic model and comparing survival against pancreatic ductal adenocarcinoma. *AJR Am J Roentgenol.* (2020) 215:390–7. doi: 10.2214/AJR.19.21921

28. Guo C, Zhuge X, Wang Q, Xiao W, Wang Z, Wang Z, et al. The differentiation of pancreatic neuroendocrine carcinoma from pancreatic ductal adenocarcinoma: the values of CT imaging features and texture analysis. *Cancer Imaging.* (2018) 18:37. doi: 10.1186/s40644-018-0170-8

29. Guo C, Zhuge X, Wang Z, Wang Q, Sun K, Feng Z, et al. Textural analysis on contrast-enhanced CT in pancreatic neuroendocrine neoplasms: association with WHO grade. *Abdom Radiol (NY).* (2019) 44:576–85. doi: 10.1007/s00261-018-1763-1

30. Kim H, An S, Lee K, Ahn S, Park DY, Kim JH, et al. Gastrointestinal pathology study group of the korean society of: pancreatic high-grade neuroendocrine neoplasms in the korean population: A multicenter study. *Cancer Res Treat.* (2020) 52:263–76. doi: 10.4143/crt.2019.192

31. Belousova E, Karmazanovsky G, Kriger A, Kalinin D, Mannelli L, Glotov A, et al. Contrast-enhanced MDCT in patients with pancreatic neuroendocrine tumours: correlation with histological findings and diagnostic performance in differentiation between tumour grades. *Clin Radiol.* (2017) 72:150–8. doi: 10.1016/j.crad.2016.10.021

32. Ohki K, Igarashi T, Ashida H, Takenaga S, Shiraishi M, Nozawa Y, et al. Usefulness of texture analysis for grading pancreatic neuroendocrine tumors on contrast-enhanced computed tomography and apparent diffusion coefficient maps. *Jpn J Radiol.* (2021) 39:66–75. doi: 10.1007/s11604-020-01038-9

33. Lam AK, Ishida H. Pancreatic neuroendocrine neoplasms: Clinicopathological features and pathological staging. *Histol Histopathol.* (2021) 36:367–82. doi: 10.14670/HH-18-288

34. Park HJ, Kim HJ, Kim JH, Kim SY, Choi SH, Byun JH, et al. Prognostic value of tumor-to-parenchymal contrast enhancement ratio on portal venous-phase CT in pancreatic neuroendocrine neoplasms. *Eur Radiol.* (2023) 33:2713–24. doi: 10.1007/s00330-022-09235-y

35. Park HJ, Kim HJ, Kim KW, Kim SY, Choi SH, You MW, et al. Comparison between neuroendocrine carcinomas and well-differentiated neuroendocrine tumors of the pancreas using dynamic enhanced CT. *Eur Radiol.* (2020) 30:4772–82. doi: 10.1007/s00330-020-06867-w

36. Elbanna KY, Jang HJ, Kim TK. Imaging diagnosis and staging of pancreatic ductal adenocarcinoma: a comprehensive review. *Insights Imaging.* (2020) 11:58. doi: 10.1186/s13244-020-00861-y

37. Granata V, Fusco R, Catalano O, Setola SV, de Lutio di Castelguidone E, Piccirillo M, et al. Multidetector computer tomography in the pancreatic adenocarcinoma assessment: an update. *Infect Agent Cancer.* (2016) 11:57. doi: 10.1186/s13027-016-0105-6

38. Shyr B-S, Shyr B-U, Chen S-C, Shyr Y-M, Wang S-E. Impact of tumor grade on pancreatic neuroendocrine tumors. *Asian J Surg.* (2022) 45:2659–63. doi: 10.1016/j.asjsur.2022.01.094

39. Azoulay A, Cros J, Vullierme MP, de Mestier L, Couvelard A, Hentic O, et al. Morphological imaging and CT histogram analysis to differentiate pancreatic neuroendocrine tumor grade 3 from neuroendocrine carcinoma. *Diagn Interventional Imaging.* (2020) 101:821–30. doi: 10.1016/j.diii.2020.06.006

40. Jiao F, Cui J, Fu D, Li Q, Wu Z, Teng Z, et al. Chinese Medical Association consensus for standardized diagnosis and treatment of pancreatic neuroendocrine neoplasms. *Chin Med J.* (2023) 136:2397–411. doi: 10.1097/CM9.0000000000002848

41. D'Onofrio M, Ciaravino V, Cardobi N, De Robertis R, Cingarlini S, Landoni L, et al. CT enhancement and 3D texture analysis of pancreatic neuroendocrine neoplasms. *Sci Rep.* (2019) 9:2176. doi: 10.1038/s41598-018-38459-6

42. Bicci E, Cozzi D, Ferrari R, Grazzini G, Pradella S, Miele V. Pancreatic neuroendocrine tumours: spectrum of imaging findings. *Gland Surg.* (2020) 9:2215–24. doi: 10.21037/gs-20-537

43. Han X, Xu X, Ma H, Ji Y, Wang D, Kuang T, et al. Clinical relevance of different WHO grade 3 pancreatic neuroendocrine neoplasms based on morphology. *Endocr Connect.* (2018) 7:355–63. doi: 10.1530/ec-17-0388

44. Saleh M, Bhosale PR, Yano M, Itani M, Elsayes AK, Halperin D, et al. New frontiers in imaging including radiomics updates for pancreatic neuroendocrine neoplasms. *Abdom Radiol (NY).* (2022) 47:3078–100. doi: 10.1007/s00261-020-02833-8

45. Singhi AD, Klimstra DS. Well-differentiated pancreatic neuroendocrine tumours (PanNETs) and poorly differentiated pancreatic neuroendocrine carcinomas (PanNECs): concepts, issues and a practical diagnostic approach to high-grade (G3) cases. *Histopathology.* (2018) 72:168–77. doi: 10.1111/his.13408

46. Gu D, Hu Y, Ding H, Wei J, Chen K, Liu H, et al. CT radiomics may predict the grade of pancreatic neuroendocrine tumors: a multicenter study. *Eur Radiol.* (2019) 29:6880–90. doi: 10.1007/s00330-019-06176-x

47. Umetsu SE, Kakar S, Basturk O, Kim GE, Chatterjee D, Wen KW, et al. Integrated genomic and clinicopathologic approach distinguishes pancreatic grade 3 neuroendocrine tumor from neuroendocrine carcinoma and identifies a subset with molecular overlap. *Mod Pathol.* (2023) 36:100065. doi: 10.1016/j.modpat.2022.100065

48. De Robertis R, Maris B, Cardobi N, Tinazzi Martini P, Gobbo S, Capelli P, et al. Can histogram analysis of MR images predict aggressiveness in pancreatic neuroendocrine tumors? *Eur Radiol.* (2018) 28:2582–91. doi: 10.1007/s00330-017-5236-7

49. Li W, Xu C, Ye Z. Prediction of pancreatic neuroendocrine tumor grading risk based on quantitative radiomic analysis of MR. *Front Oncol.* (2021) 11:758062. doi: 10.3389/fonc.2021.758062

50. Hilabi BS, Alghamdi SA, Almanaa M. Impact of magnetic resonance imaging on healthcare in low- and middle-income countries. *Cureus.* (2023) 15:e37698. doi: 10.7759/cureus.37698

51. Murali S, Ding H, Adedeji F, Qin C, Obungoloch J, Asllani I, et al. Bringing MRI to low- and middle-income countries: Directions, challenges and potential solutions. *NMR BioMed.* (2024) 37:e4992. doi: 10.1002/nbm.4992

52. Granata V, Fusco R, Sansone M, Grassi R, Maio F, Palaia R, et al. Magnetic resonance imaging in the assessment of pancreatic cancer with quantitative parameter extraction by means of dynamic contrast-enhanced magnetic resonance imaging, diffusion kurtosis imaging and intravoxel incoherent motion diffusion-weighted imaging. *Therap Adv Gastroenterol.* (2020) 13:1756284819885052. doi: 10.1177/1756284819885052

53. Mo S, Yi N, Qin F, Zhao H, Wang Y, Qin H, et al. EUS-based intratumoral and peritumoral machine learning radiomics analysis for distinguishing pancreatic neuroendocrine tumors from pancreatic cancer. *Front Oncol.* (2025) 15:1442209. doi: 10.3389/fonc.2025.1442209

54. Xie N, Fan X, Chen D, Chen J, Yu H, He M, et al. Peritumoral and intratumoral texture features based on multiparametric MRI and multiple machine learning methods to preoperatively evaluate the pathological outcomes of pancreatic cancer. *J Magnetic Resonance Imaging.* (2023) 58:379–91. doi: 10.1002/jmri.28538

55. Chen L, Yuan M, Wang M, Luo C, Gao M, Wan Y, et al. Comparison between pancreatoblastoma (PB) and solid pseudopapillary neoplasm (SPN) in pediatric patients with enhanced CT. *Pancreatology.* (2024) 24:1152–9. doi: 10.1016/j.pan.2024.09.014

56. Wang M, Chen W, Ren R, Lin Y, Tang J, Wu M. Comparative analysis of multi-zone peritumoral radiomics in breast cancer for predicting NAC response using ABVS-based deep learning models. *Front Oncol.* (2025) 15:1586715. doi: 10.3389/fonc.2025.1586715